HortScience 60(6):920–930. 2025. https://doi.org/10.21273/HORTSCI18564-25

# Research of Adsorption Experiments and Coupled Simulation of Multi-scale Flexible Tea Leaves

**Zhang Xu**
*Huzhou Vocational and Technical College, College of Intelligent Manufacturing and Elevator, Huzhou 313000, China*

**Xinyu Zhu**
*Huzhou Vocational and Technical College, College of Continuing Education, Huzhou 313000, China*

**Wei Jiao**
*Chinese Academy of Agricultural Sciences, Grassland Research Institute, Hohhot 010010, China*

**Zhongyou Zhou**
*Huzhou Vocational and Technical College, College of Intelligent Manufacturing and Elevator, Huzhou 313000, China*

*Keywords.* adsorption test, CFD-DEM coupling model, motion trajectory, negative pressure flow field

***Abstract.*** **To develop a new type of air suction sorting equipment for tea, we performed a bench test using a high-speed camera for test shooting and data analysis and established a computational fluid dynamics–discrete element method (CFD-DEM) coupling model. The experimental results showed that under the same negative pressure and the initial fall distance from the adsorption surface, the multiscale tea leaves (collectively referred to as leaves) were adsorbed in the air suction flow field in different tracks, and the greater the mass difference of leaves, the greater the difference in their movement tracks. By using this feature, the multiscale machine-picked tea could be separated under the same negative pressure. The CFD-DEM coupling model was used to simulate and fit the motion locus points of the leaves in the same negative pressure flow field with different initial distance from the negative pressure adsorption surface. The results showed that the distance between the falling position of the leaves and the bottom of the negative pressure adsorption surface was proportional to the initial fall distance. The distance between the adsorbed leaves and the bottom of the negative pressure adsorption surface was inversely proportional to the initial fall distance. In summary, this research provides theoretical support for the future development of sorting equipment with suction for tea leaves.**

Tea picking has always been a key and difficult part of tea mechanization and a key link that restricts large-scale tea production. Since the early 1950s in China, machine-picking tests have been used for mass tea picking; the efficiency of machine-picking tea is much higher than that of manual labor, and the cost is effectively reduced (Wu 2022). However, machine-picked tea often has irregular leaves; therefore, it needs to be sorted during processing. We selected an air suction sorting method for machine-picked tea. Air suction technology mainly uses the principle of suction generated by negative air pressure to realize the adsorption of objects, transportation, and other operations. In agricultural engineering applications, a negative pressure environment is usually generated by air pumps and other equipment so that gas flows in specific pipelines or components to form suction, thus acting on agricultural production (Cui et al. 2017; Jiang et al. 2019).

Air suction technology is applied to the field of seeding and includes air suction precision seeders and the use of negative pressure to absorb the seeds on the suction hole of the seed tray; with the rotation of the seed tray, the seeds are accurately placed in the seed ditch (Li et al. 2022; Mu et al. 2022; Zhao et al. 2020). Air suction seeding equipment has also been applied in the process of seedling rearing in the vegetable hole tray, which can more accurately suck-up tiny vegetable seeds and plant them in the seedling holes in the hole tray, thus ensuring the accuracy of the number of seeds in each hole (Luo et al. 2010; Xiao 2023; Xu and Chen 2022). Suction technology is also used in the field of harvesting. For some fruits and vegetables, the air suction picker has played an important role; through the design of a suitable suction nozzle and suction control system, mature fruits and vegetables from the plant can be gently sucked and transported to collection device (Ji et al. 2017; Ju 2022; Zhang 2024; Zhang et al. 2020). In terms of harvest and impurity removal, air suction technology can be used for cleaning and conveying links, and the use of air suction sucks away the mixed light debris such as glume shell and straw debris. In summary, this research showed that the pneumatic suction has been widely used in the agricultural field, and its advantages are mainly reflected in improving agricultural production efficiency and improving the quality of agricultural products and precision operations.

With the rapid development of computer technology, computational fluid dynamics–discrete element method (CFD-DEM) coupling simulation technology has gradually become an important tool in agricultural engineering research that can accurately describe complex phenomena such as multiphase flow and particle movement involved in agricultural production processes and provide strong support for optimal design and scientific research of agricultural engineering (Chen et al. 2024; Kong 2023; Zhang 2021). In the field of agricultural material handling, CFD-DEM coupled simulation can be used to study the movement of seeds in parts such as seed feeders and seed delivery tubes (Li et al. 2021; Zhang et al. 2020). For harvesting machinery, such as combine harvesters, CFD-DEM coupling simulation can be used to analyze the motion state of grain during threshing and cleaning (Chen 2021; Yuan et al. 2023; Zhao 2020). In terms of storage, CFD-DEM coupling simulation can simulate the accumulation form and ventilation effect of agricultural materials such as grains in the warehouse and analyze the influence of different storage layouts and ventilation methods on the storage quality of materials (Chen et al. 2022; Gou 2021; Xie 2023; Zhou 2021). The characteristics of fluid flow and particle movement trajectory in the flow field are simulated to design and optimize agricultural machinery (Zhang et al. 2024a, 2024b). In summary, this research showed that the application of CFD-DEM can more truly describe complex phenomena, provide the basis for optimal design, and reduce the test cost and time.

In the field of agricultural engineering, scholars have conducted ample research of the use of air suction and have obtained good

Received for publication 4 Mar 2025. Accepted for publication 4 Mar 2025.
Published online 13 May 2025.
This work was supported by the Natural Science Foundation of Huzhou Science and Technology Bureau (2023YZ51), Inner Mongolia Natural Science Foundation (2023LHMS05045), and Huzhou Science and Technology Bureau public welfare fund project (2021GZ27).
The authors have no conflict of interest to declare regarding this study or its findings.
The data that supports the findings of this study are available on request from the corresponding author.
Z.X. is the corresponding author. E-mail: z_xu1987@163.com.

test results. However, regarding the operation process of air suction equipment, it is necessary to continuously consume electric energy or other energy to maintain the operation of the air pump to generate suction, and this energy consumption is relatively large. However, in multiscale tea leaf processing, after the use of air suction to separate tea leaves, the generated air suction flow can be further processed for drying, tail adjustment, and air impurity removal, to fully use the energy and reduce energy waste.

We performed the motion trajectory test of multiscale flexible leaves using the air suction model and established the coupling model of discrete element method and computational fluid dynamics (CFD-DEM) of material particle motion in the negative pressure flow field. The coupling model was used to analyze the motion trajectory of leaves in the same negative pressure flow field and at different initial multiscale falling positions. Thus, better design parameters are provided for the research and development of multiscale suction sorting equipment for tea.

## Multiscale Leaf Falling and Adsorption Experiments

### Test materials and methods

*Flexible blade parameter measurements.* The purpose of this experiment was to test the differences in the motion trajectories of leaves with different masses when they were affected by the air suction flow field during the falling process. A scientific research balance (Wante Weighing Instrument Co., Ltd., Jiangsu, China) with a measurement accuracy of 0.001 g was used to measure the masses of 40 selected leaves. After measurement was performed, the masses of the leaves were classified. Then, considering the characteristics of the leaf contours and masses, three leaves with certain mass differences were selected as the test leaves. Among them, the maximum mass was 1.052 g, the minimum mass was 0.206 g, and the mass of leaf 2, which was the comparative test leaf, was 0.35 g (Fig. 1).

*Bench test.* The bench test was built (Fig. 2) to test the multiscale analysis of the leaf falling motion and trajectory. The bench test comprised a negative pressure fan (Foshan Mi Wind Electrical Equipment Co., Ltd., Foshan City, Guangdong, China), conveyor belt (assembly equipment), measuring plate, and high-speed camera (Hunan Ketian Technology Co., Ltd., Changsha City, Hunan, China). The suction tuyere of the negative pressure fan had a diameter of 200 mm, the wind pressure was 340 Pa, and the air volume was 1200 $m^3$/h. The width of the conveyor belt was 200 cm, and the transmission speed of the conveyor belt could be adjusted by the speed regulating motor. The speed of the conveyor belt in this study was constant. The 10-$mm^2$ measuring plate was convenient for observing the fall and adsorption of leaves. The high camera combination was composed of a high-speed camera, industrial computer, and light source. The shooting exposure time of the high-speed camera was 270 $\mu$s, the shooting frame rate was up to 3518 Fps, and the shooting resolution was 1280 × 860.


Fig. 1. Leaf quality measurement.

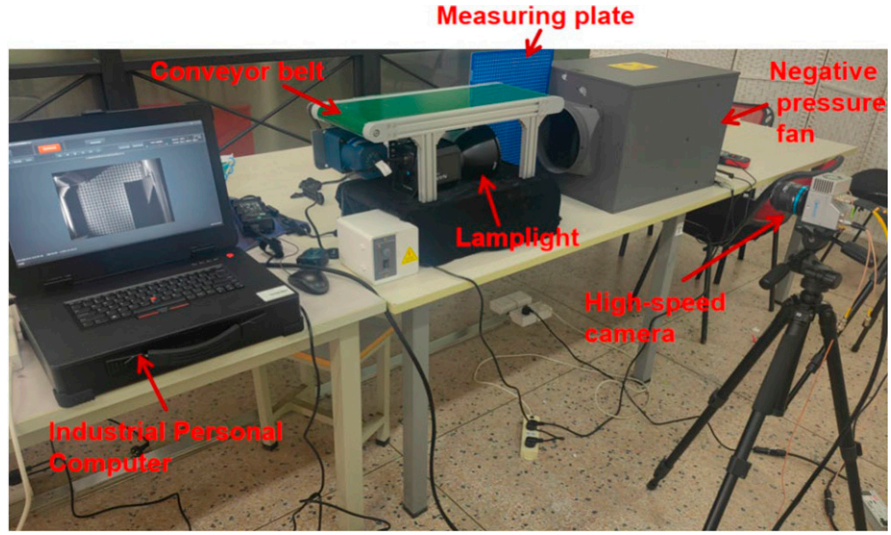


Fig. 2. Bench test of leaf air absorption.

*Test methods.* The leaves were placed at a certain interval on the conveyor belt, and the distances between the end of the conveyor belt and the suction tuyere of the negative pressure fan were 150 mm, 110 mm, 80 mm, and 30 mm. The distance between the conveyor belt and the negative pressure fan was used as the background of the measuring plate, which was convenient for describing the multiscale leaf falling movement trajectory. After starting the conveyor belt, the motion track of the falling leaves was recorded with a high-speed camera, several measurements were performed, and a group with stable results was selected as the analysis object.

### Test analysis

To describe the movement trajectory of leaves, the point displayed as "8" on the upper right scale of the mapping board was considered the starting point, and the "8" scale in the downward direction was defined as the increasing scale value, which was defined as the coordinate y-axis. The "8" scale in the direction of the conveyor belt was also defined as the increasing scale value and defined as the x-axis, with the coordinates at the position of the center of the leaf considered the position point of the leaf. Using the coordinate points, the trajectory of leaf adsorption and the suction wind force of leaf adsorption points in the future were reflected, resulting in an improved analysis of mechanical properties of leaves in the air field.

*Motion trajectory of leaf 1 under the negative pressure flow field.* Figure 3 shows the fall adsorption movement of leaf 1. Figure 3A shows the leaf falling from the conveyor belt, and its coordinate value was (27 cm, 12 cm). Because of the suction effect of the negative pressure flow field, the leaves did not fall freely; instead, they moved toward the negative pressure adsorption port (Fig. 3B), where the coordinate values of the leaves were (25 cm, 17 cm). With the fall of leaves, the suction speed of negative pressure air increased, and the leaves moved more toward the tuyere of the negative pressure fan (Fig. 3C), where the coordinates of leaves were (22 cm, 22 cm). Based on the changes noted in Fig. 3D and 3E, although the leaves were affected by the negative pressure adsorption air flow (Fig. 3D), they still fell downward when moving (Fig. 3E) and were not horizontally adsorbed. According to our previous analysis of the flow field pneumatics of the negative pressure tuyere, the negative pressure suction generated by the suction tuyere of the negative pressure fan had a certain dispersion. Therefore, a certain pushing force on the downward movement of the leaves occurred, so that the adsorption force could not overcome the gravity of the leaves itself and the weight distribution of the leaves was uneven, resulting in the inability of the suction to act uniformly on the entire leaves and affecting the adsorption effect. The coordinates of the leaves in Fig. 3D and 3E were (19 cm, 26.5 cm) and (16.5 cm, 30 cm), respectively. In Fig. 3E and 3F, the leaves were sucked horizontally into the negative pressure air outlet, indicating that the air suction force on the leaves was greater than the gravity force of the leaves, and the leaves were sucked directly. The coordinates of these leaves were (14 cm, 31 cm).

In conclusion, during the process of falling, leaves were affected by air suction and gravity,

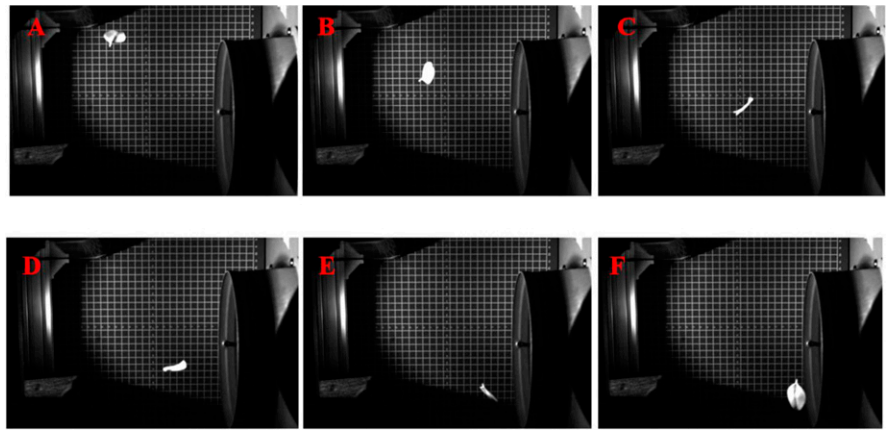


Fig. 3. Movement trajectory of leaf 1 during the adsorption process.

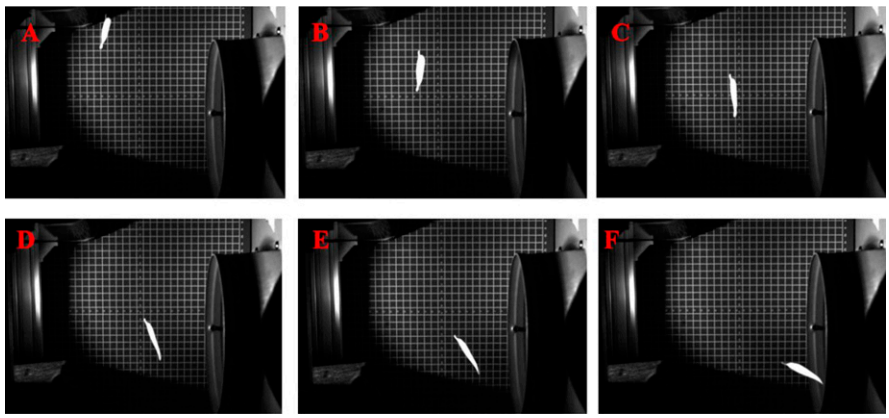


Fig. 4. Movement trajectory of leaf 2 during the adsorption process.

causing them to fall and move toward the negative pressure tuyere. Under this test condition, leaves were mainly affected by gravity and fall from a height until they were absorbed. The acceleration of gravity gradually increased the falling speed of leaves until they were stopped by the force of the adsorption port and the leaves were absorbed. Under the mass of the leaves (0.206 g), when the tuyere was 30 mm and the suction wind speed was 6.17 m/s, the leaves were directly adsorbed.

*Motion trajectory of leaf 2 under the negative pressure flow field.* Figure 4 shows the falling and adsorption process of leaf 2. There was a mass difference of 0.144 g between leaf 2 and leaf 1. The surface area of leaf 1 was larger than that of leaf 2. Such morphological differences affect the air resistance and stability of the leaves during the falling process. During the falling process of the leaves, their aerodynamic performance had a significant impact on the falling shape. The mass difference of the leaves lead to changes in aerodynamic performance, which, in turn, affected the morphological features such as the stability and rotation during the falling process. Therefore, there were certain differences in the falling shapes between leaf 2 and leaf 1.

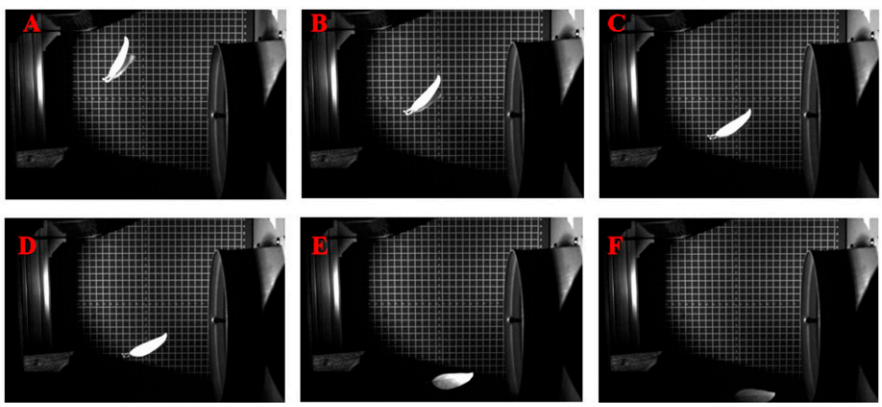


Fig. 5. Movement trajectory of leaf 3 during the adsorption process.

Figure 4A shows the state of falling leaves with coordinates of (27 cm, 11 cm). As the leaves fell, because of the influence of the negative pressure air flow field, they moved closer to the negative pressure tuyere; the coordinates of the leaves at this position were (25 cm, 17 cm) (Fig. 4B) and (23.5 cm, 20.5 cm) (Fig. 4C). Figure 4D and 4E show that leaves were affected by negative pressure air suction, and that the surface of leaves was affected by negative pressure suction. The falling head of leaves tended to rotate and lift toward the negative pressure tuyere, and the coordinates of these leaves were (20.5 cm, 24.5 cm) (Fig. 4D) and (17.5 cm, 26 cm) (Fig. 4E). During the process of negative pressure adsorption, the air force on the leaves was not uniform, which lead to the rotation of the leaves. The geometric shape and mass distribution of the leaves resulted in an uneven flow rate and uneven pressure of the air flow on the surface of the leaves, resulting in torque that caused the head of the leaves to turn to the tuyere.

*Motion trajectory of leaf 3 under the negative pressure flow field.* Figure 5 shows the fall adsorption process of leaf 3. Figure 5A shows the initial fall position of leaf 3 with coordinates of (26 cm, 16 cm). With the fall of leaves and adsorption of the negative pressure tuyere, leaf 3 moved closer to the negative pressure tuyere; however, compared with leaf 1 and leaf 2, the adsorption distance of leaf 3 was smaller (Fig. 5B–5D), with motion coordinates of (25 cm, 21 cm), (23.5 cm, 25 cm), and (22 cm, 27 cm). In Fig. 5A and 5D, the adsorption distance of leaf 3 by the negative pressure tuyere was 4 cm, and the adsorption distances of leaf 1 and leaf 2 at the same position were 10.5 cm and 9 cm. In Fig. 5E and 5F, leaf 3 was not adsorbed by the negative pressure tuyere, and the motion coordinates were (20 cm, 32 cm) and (19 cm, 33.5 cm), respectively. Leaf 3 was not adsorbed by the negative pressure tuyere because the weight of the leaves was large, and the gravity of the leaves was always greater than the adsorption force of the negative pressure tuyere; therefore, it was not adsorbed.

*Comparative analysis of falling tracks of three types of leaves.* The coordinate system (Fig. 6A) was established with mapping board "8" as the origin of coordinates and the falling area of leaves as the third quadrant of the coordinate axis; therefore, the corresponding coordinates (x and y) were negative (the spacing between the ruler plates was 1 cm). Trace lines were drawn for the coordinates of the positions of these three types of leaves in the process of falling (Fig. 6B). According to the trace lines of the three types of leaves, leaf 1 and leaf 2 had relatively similar trace lines when falling, there was a large separation at coordinates (−20.5 cm, −24.5 cm), and the maximum difference in longitudinal positions was 7 cm. The maximum difference in the longitudinal position between the two was 3 cm. The mass difference between leaf 1 and leaf 2 was 0.144 g; however, when the two leaves were falling, the shape of the leaves was quite different, so they were subjected to different

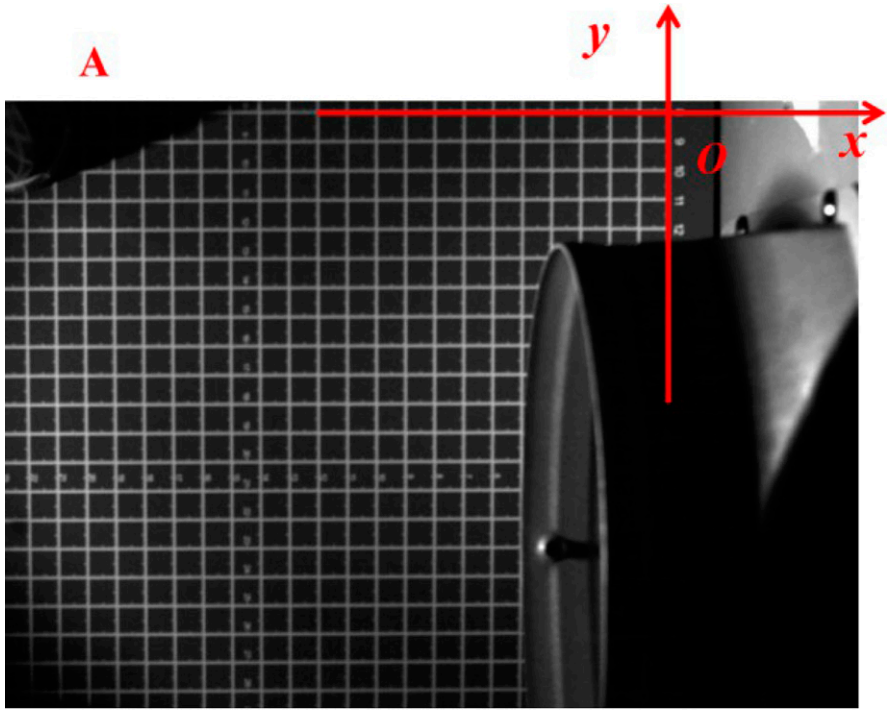


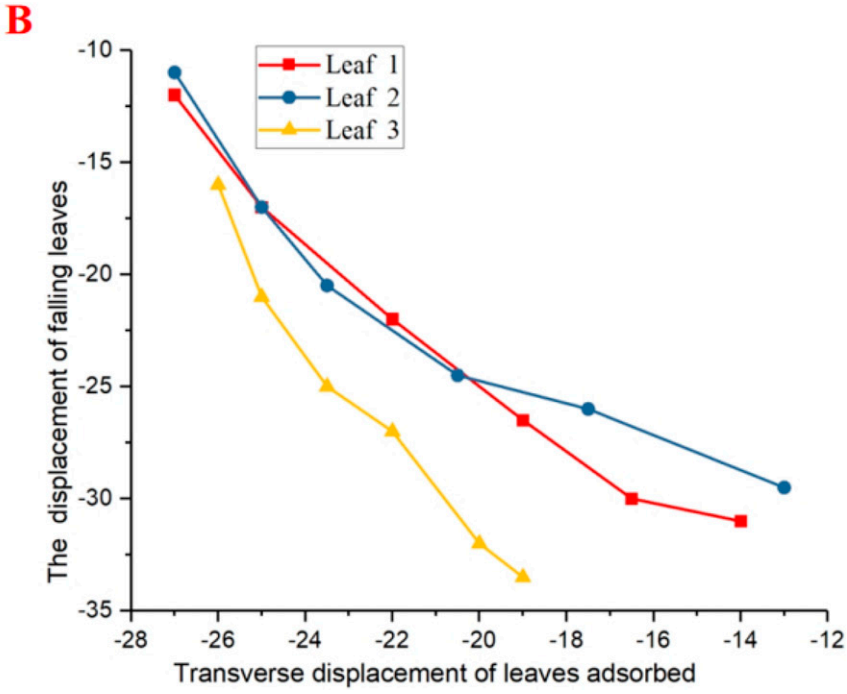


Fig. 6. Establishment of coordinate system and description of the leaf motion trajectory.

air resistance during the falling process. The symmetry of leaf 2 was better than that of leaf 1; therefore, the posture of leaf 2 was more stable during the falling process, whereas leaf 1 produced a certain tumbling phenomenon, resulting in the constant change of the adsorption surface of leaf 1. The falling posture of leaf 2 was stable, and the affected area of the adsorbed air was stable; therefore, it will be adsorbed by the air suction field in advance.

Under the adsorption effect of negative pressure, the movement trace of leaf 3 toward the negative pressure air outlet was smaller than that of leaf 1 and leaf 2, and the falling trajectory of leaf 3 was more similar to an inclined straight line. There was no trend of movement like that of the negative pressure air outlet because the mass of leaf 3 was greater than that of leaf 1 and leaf 2, and the direction of the resultant force of leaf 3 was the direction of the combination of gravity and negative pressure suction. Therefore, a sloping straight fall occurred because of the large mass and the negative pressure suction was not enough to change its tendency to fall mainly with gravity.

In summary, the experimental study showed that the leaves with certain quality differences can be sorted by negative pressure adsorption. Because the origin of the coordinates was "8" and the distance between the negative pressure tuyere and the origin was 5 cm, the horizontal coordinate dimensions in Fig. 6B include the aforementioned distance; therefore, it could be determined that leaf 3 falls at the transverse distance of 5 cm from the negative pressure tuyere and was not adsorbed.

## Establishment and Verification of the Coupling Model Based on CFD-DEM

### Governing equation of the coupled model

Fluid flow needs to follow the conservation of mass, conservation of momentum, and conservation of energy laws. If the fluid is in turbulent motion, then it also needs to follow the turbulent transport equation. The governing equation is a mathematical way to describe these laws. This chapter mainly studies the motion of the external air flow field under the influence of the intake and intake flow of the porous rotary table, and now regards the air flow as an incompressible, viscous, turbulent and adiabatic fluid, satisfying the mass conservation equation and the momentum conservation equation.

$$\frac{\partial}{\partial x_i}(\rho\mu_i) = 0 \qquad [1]$$

where $\mu_i$ is the velocity component of air in the direction $i$.

The momentum conservation equation can be described as follows:

$$\frac{\partial}{\partial x_i}(\rho\mu_i\mu_j) = -\frac{\partial H_j}{\partial x_i} + \frac{\partial \tau_{ij}}{\partial x_i} + F_i \qquad [2]$$

where $H_j$ is static pressure, $\tau_{ij}$ is stress tensor, and $F_i$ is volume force.

In this study, the Realizable k-$\varepsilon$ turbulence model was used for model calculations and is suitable for complex shear flows involving fast strain, medium vorticity, and local transition, with high accuracy. The transport equations of $k$ and $\varepsilon$ in the Realizable $k$-$\varepsilon$ model are as follows:

$$\frac{\partial(\rho\mu_j\varepsilon)}{\partial x_j} = \left(\mu + \frac{\mu t}{\sigma_\varepsilon}\right)\nabla^2\varepsilon + C_1 S\rho\varepsilon - C_2\frac{\rho\varepsilon^2}{k+\sqrt{\nu\varepsilon}} \qquad [3]$$

where $\mu$ is hydrodynamic viscosity, $C_1 = \max\left[0.43, \frac{\gamma}{\gamma+5}\right]$, $C_2 = 1$, $\sigma_\varepsilon = 1.2$, and $\nabla$ is a Laplace operator.

The governing equation of the particle at any time is as follows:

$$m_i\frac{dv_i}{dt} = m_i g + f_{drag,i} \qquad [4]$$

$$I_i\frac{dw_i}{dt} = \sum_{j=1}^{k_i} T_{ij} \qquad [5]$$

where $m_i$, $v_i$, $w_i$, and $I_i$ are the mass, velocity, angular velocity, and moment of inertia of the particle, $k_i$ is the number of colliding particles, $T_{ij}$ is particle torque,

Table 1. Parameters required in discrete element method simulation.

| Parameter | Value |
|---|---|
| Poisson's ratio of tea leaves | 0.45 |
| Density of tea leaves (kg/m$^3$) | 840 |
| Shear modulus of tea leaves (Pa) | 3.3e+06 |
| Poisson's ratio of equipment | 0.45 |
| Density of equipment (kg/m$^3$) | 950 |
| Shear modulus of equipment (Pa) | 3.2e+0.7 |
| Tea leaves—tea leaves restitution coefficient | 0.7 |
| Tea leaves—tea leaves static friction coefficient | 0.85 |
| Tea leaves—tea leaves rolling friction coefficient | 0.07 |
| Tea leaves—equipment restitution coefficient | 0.07 |
| Tea leaves—equipment | 0.75 |
| Tea leaves—equipment rolling friction coefficient | 0.06 |

$m_i g$ is particle gravity, and $f_{drag,i}$ is the drag force of fluid.

## Coupling simulation settings

*Discrete element settings.* Material properties of three types of leaves were added, and the relevant parameters of leaves in this experiment were determined by referring to the test methods and relevant data of leaf physical parameters reported previously (Li et al. 2024; Zhang et al. 2024b) (Table 1). By analyzing these test data, it was found that the motion tracks of leaf 1 and leaf 2 are similar (Fig. 6B). Therefore, to simplify the calculation of the simulation model, the discrete element model was defined as two particles with different qualities, and the average mass of the two leaves was selected to define the mass of discrete element particle 1, that is, 0.278 g (see Fig. 1 for the mass of two leaves). The other particle had a mass of 1.052 g. Create a virtual particle factory plane, the dimension of the plane length/width was 200 mm/6 mm, the distance between the center line of the plane width of the particle factory and the distance between the width of the particle factory and the negative pressure tuyere was 150 mm, and the distance between the particle factory and the width of the negative pressure tuyere was 170 to 130 mm, the number of particles falling per second of the three particles was 1000, and the falling speed was 0.5 m/s. Particles fall straight down in the direction of gravity. The "particle to particle" interaction between particles was selected, and the Bonding V2 application model was selected. The discrete element solution time step was 1e-05 s, and the total solution time was 1 s.

*Boundary conditions for CFD meshing and division.* The ICEM module of CFD was used to divide the computing domain into grids. The grids were tetrahedrons and the number of grid elements was 275,000. The mesh quality evaluation criteria were based on the minimum orthogonal mass, maximum aspect ratio, and maximum orthogonal slope (Fig. 7).

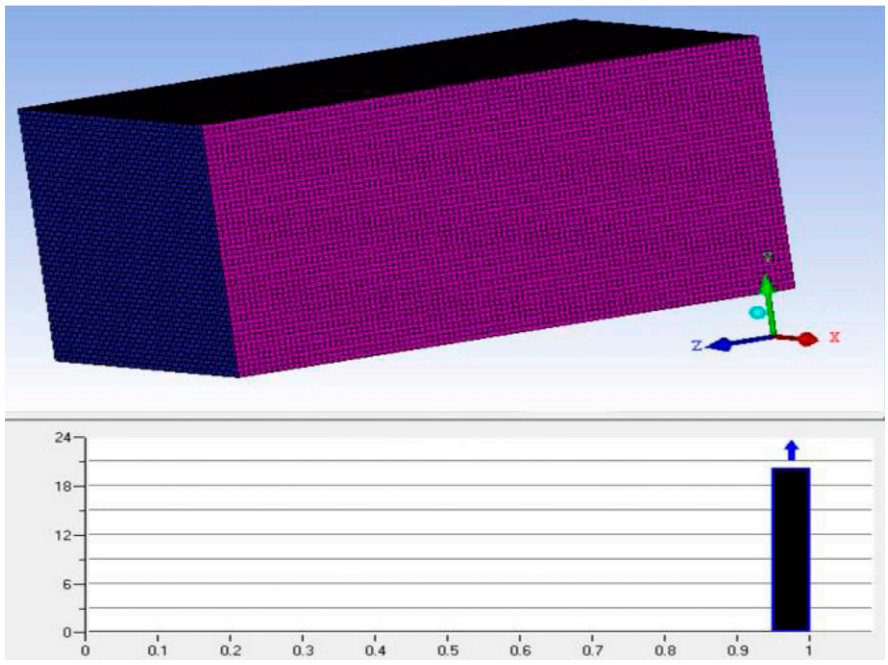


Fig. 7. Mesh division and mesh quality of the fluid region.

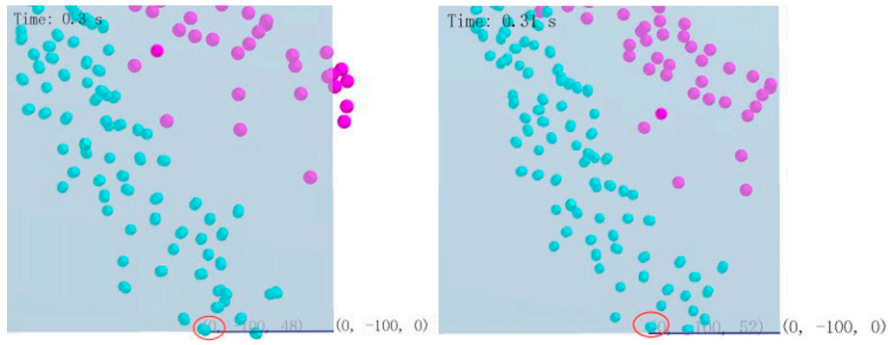


Fig. 8. Simulation verification.

In the numerical simulation, the influence caused by heat exchange was ignored, that is, the energy equation was not considered. The flow field belonged to turbulent flow, the working medium was air, there was no phase change, and there was no chemical reaction in the calculation process. A separate implicit solver based on pressure was used to solve the numerical simulation. To improve the calculation accuracy and reduce the numerical diffusion, the momentum, turbulent kinetic energy, and turbulent dissipation rate were adopted in the second-order upwind discrete scheme. The pressure-velocity coupled SIMPLEC algorithm was selected. The working environment was set to standard atmosphere. The inlet boundary condition was set to pressure-inlet, the outlet boundary condition was set to pressure-outlet, the pressure was −340 Pa, and the backflow turbulence intensity was 5%.

## Simulation verification

Fig. 8 shows the simulation and verification results of the CFD-DEM coupling model built, in which the mass of the "cyan" particle was 1.052 g and that of the "magenta" particle was 0.278 g. After 0.3 s of simulation, the negative pressure flow field reached a stable state, the particles were adsorbed, and the adsorption track line was similar to that in Fig. 6B. The "cyan" particles were selected within the simulation time, and the last position that was not adsorbed was selected. To reduce the difference, the particles in the center position of particle engineering, that is, the particles 150 mm away from the adsorption surface, were selected, and four were selected for distance measurements. The transverse distances of the final unadsorbed position from the negative pressure adsorption surface were 48, 48, 52, and 52 cm, respectively, and the error range of the test distance was 4%. In summary, the error between the particle simulation results and the experiment was less than 5%, which showed that the model was correct and applicable.

In the initial stage of simulation, it was found that particles were not directly adsorbed; instead, they were slowly adsorbed by negative pressure. As shown in Fig. 9, from 0.15 to 0.16 s, "magenta" particles are

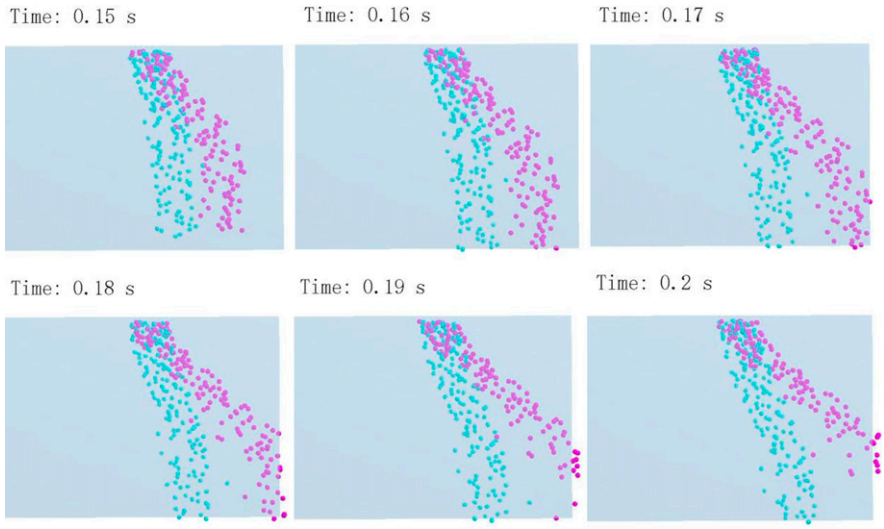


Fig. 9. Motion state of particles before adsorption.

not adsorbed; instead, they fall directly. At 0.17 to 0.18 s, the "magenta" particles were gradually adsorbed by the negative pressure surface. With progression of the simulation, the negative pressure value gradually stabilized. At 0.19 to 0.2 s, the position of "magenta" particles adsorbed gradually became similar to the trajectory of leaf 1 and leaf 2 in the test, that is, they were adsorbed by the negative pressure port. "Cyan" particles were the heavier particles in this simulation. Through the movement between 0.15 and 0.2 s, it was found that the particles were initially less affected by the adsorption flow field, and that the particles fell almost vertically. As the adsorption flow field gradually stabilized, the motion state of the particles reached a stable state, that is, they leaned toward the negative pressure air outlet, but were not adsorbed. In summary, the simulation showed that in the initial stage of negative pressure adsorption, the negative pressure air flow did not reach a stable state, which affected the adsorption efficiency of leaves. After the air flow field is stable, leaf adsorption can occur.

## Multiscale Leaf Adsorption Trajectory Analysis

Through the aforementioned experiments and simulations, it was found that the leaves were adsorbed differently under different negative pressure air field environments, different leaf masses, and different fall distances from the adsorption surface. In the previous stage, the particle adsorption trajectory under different negative pressure flow fields with the same mass was studied (Zhang et al. 2024a). Based on that study, we simulated and analyzed the single-factor variables with different distances between leaf fall and adsorption surface and different negative pressure flow field environments.

The established CFD-DEM coupling simulation model was used to analyze and define multiscale leaves, and the mass was set as 1.6, 1.3, 0.3, and 0.1 g, the negative pressure value was a constant 340 Pa, and the initial distances between the fall of leaves and the negative pressure adsorption surface were 160, 140, 120, 90, 70, and 50 mm. The adsorption surface length was 200 mm, and the leaf adsorption analysis was conducted.

### Motion trajectory and analysis of leaves with a mass of 1.6 g in a negative pressure flow field

Figure 10A shows the minimum distance between the unadsorbed position and the adsorption surface when the leaf mass of 1.6 g (selection default) fell with a different initial distance from the negative pressure adsorption surface. The particles of this mass were never adsorbed under the conditions of this study, but their movement trajectory indicated that they tended to move toward the adsorption surface under the action of the negative pressure airflow field. The lower end of the adsorption surface was selected as the starting point of ranging, and the middle line of the particle motion path was the endpoint of ranging. The distance between the final position of the particle that was not adsorbed and the endpoint under the negative pressure adsorption surface were 138, 110, 92, 59, 43, and 25 mm, and the coordinates composed of the initial position of the particle fall were (160 cm, 138 cm), (140 cm, 110 cm), (120 cm, 92 cm), (90 cm, 59 cm), (70 cm, 43 cm), and (50 cm, 25 cm), respectively.

The initial distance between the falling leaf and the negative pressure adsorption surface was considered the x-axis, and the distance between the final position of the particle not adsorbed and the endpoint below the negative pressure adsorption surface was considered

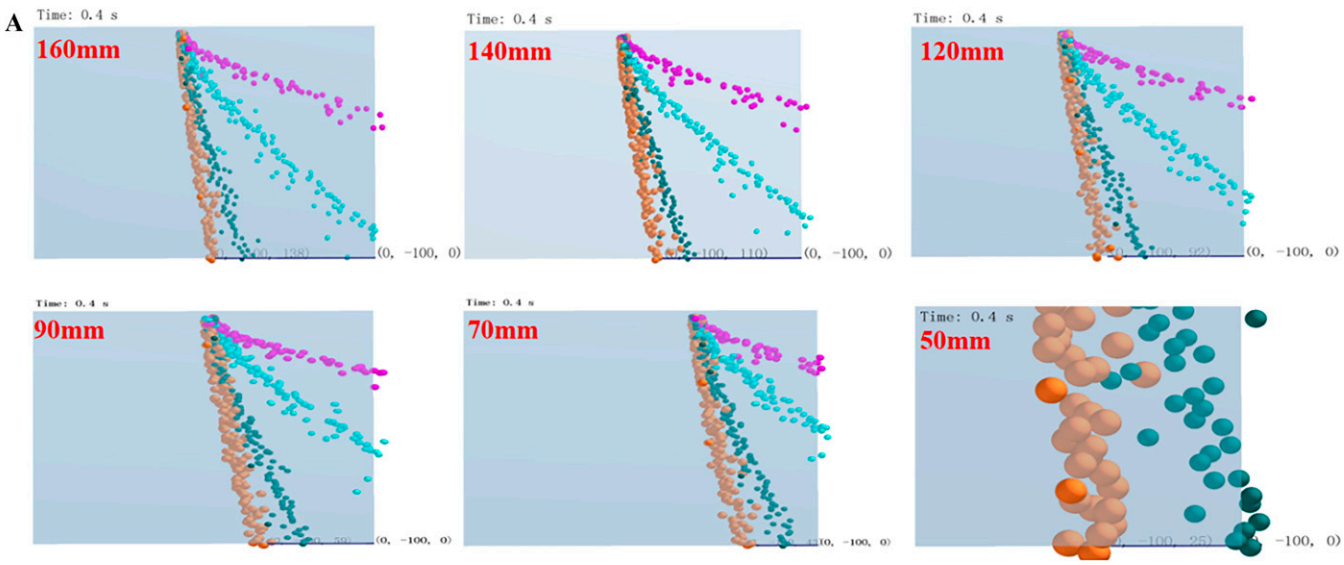


Fig. 10. (**A**) When the weight of leaves is 1.6 g and the initial distance between the falling position and the negative pressure adsorption surface is different, the final falling position and adsorption surface are the minimum distance. (**B**) The functional relationship between the leaf mass of 1.6 g, initial fall position of the leaf, and distance between the unadsorbed place and adsorption surface.

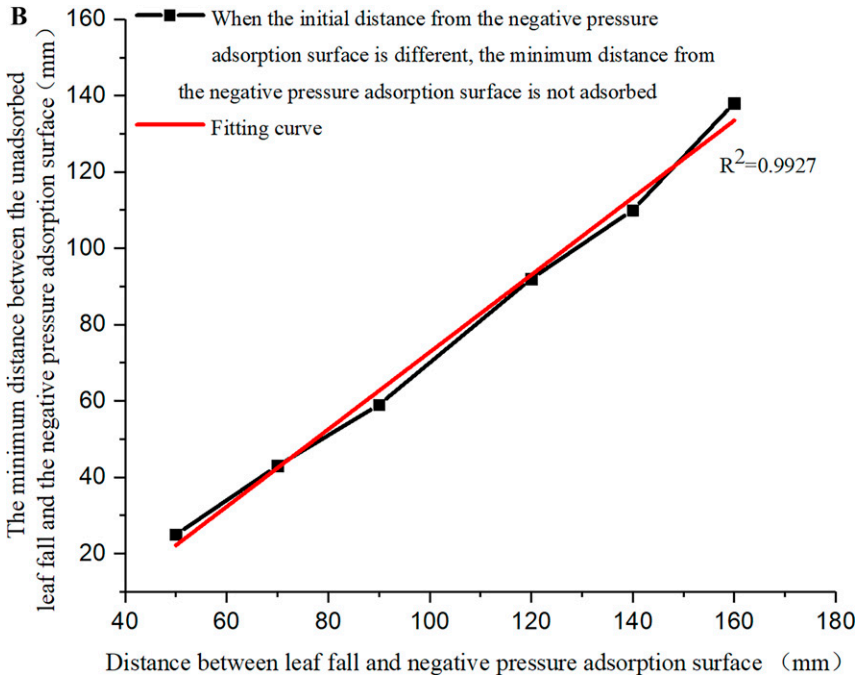


Fig. 10. Continued

the y-axis. The scatter plot was established, function fitting was performed on the scatter plot (Fig. 10B), the fitting function expression was $y = -28.40 \pm 4.33 + (1.01 \pm 0.04)x$, and the adjusted $R^2$ of the fitting function was 0.9927, which indicated that the fitted function (model) sufficiently captured the law in the data and had a strong ability to explain the change of the dependent variable. According to the fitting function, there was a relatively obvious linear correlation trend between the two variables studied. The positive slope of the fitting function indicated that the two variables were positively correlated, that is, when the value of one variable increased, the value of the other variable also tended to increase. In other words, at this mass, the initial position of the leaves falling from the negative pressure adsorption surface was larger. The leaves fall further away from the negative pressure adsorption surface.

### Motion trajectory and analysis of leaves with mass of 1.3 g in a negative pressure flow field

Figure 11A shows the minimum distance between the unadsorbed position and the adsorption surface when the leaf mass of 1.3 g (dark cyan) falls at different initial distances from the negative pressure adsorption surface. It can be seen from the particle movement trajectory that under the simulated environment under this condition, the particles of this mass were not adsorbed at an initial distance of no less than 70 mm from the negative pressure adsorption surface. At the initial distance of 50 mm from the negative pressure adsorption surface, the particles were adsorbed just at the bottom of the adsorption surface with a height of 200 mm. When the particles with this mass moved to the bottom, the distances from the bottom of the negative pressure adsorption surface were 107, 89, 66, 40, 20, and 0 mm, and the coordinates formed by the initial position of the particle fall were (160 cm, 107 cm), (140 cm, 89 cm), (120 cm, 66 cm), (90 cm, 40 cm), (70 cm, 20 cm), and (50 cm, 0 cm), respectively.

Similarly, the initial distance from the negative pressure adsorption surface when the leaf falls was considered the x-axis, and the distance from the final position of the particle not adsorbed to the lower end of the negative pressure adsorption surface was considered the y-axis. The scatter plot was established, and function fitting was performed on the scatter plot (Fig. 11B); the fitting function expression was $y = -48.28 \pm 1.65 + (0.97 \pm 0.01)x$, and the adjusted $R^2$ of the fitting function was 0.9989. The fitted function (model) sufficiently captured the law in the data and had a strong ability to explain the change of the dependent variable. At this mass, there was a linear positive correlation between the initial falling distance and the distance from the bottom of the adsorption surface.

### Motion trajectory and analysis of leaves with mass of 0.3 g in a negative pressure flow field

Figure 12A shows the leaf mass of 0.3 g (cyan). When the leaf fell at different initial distances from the negative pressure adsorption surface, the particles were adsorbed by the negative pressure adsorption surface, with the center of the adsorption surface as the starting point. Particles of this mass fell 160 mm

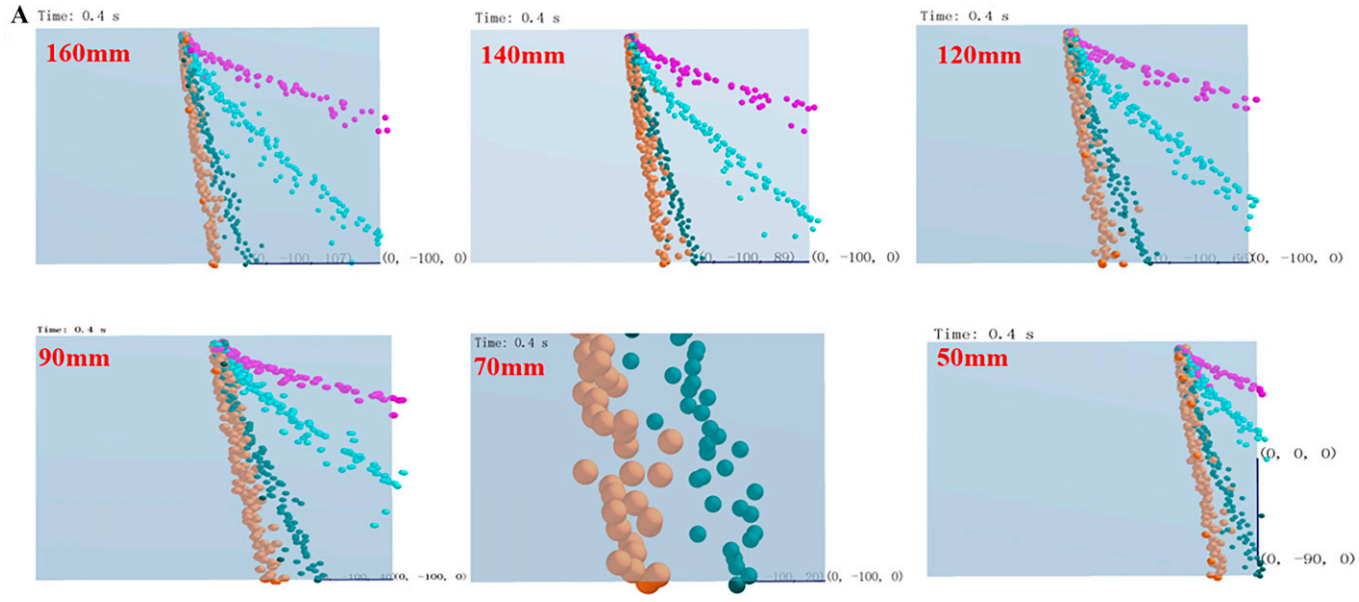


Fig. 11. (**A**) When the weight of leaves is 1.3 g and the initial distance between the falling position and negative pressure adsorption surface is different, the final falling position and adsorption surface are the minimum distance. (**B**) The functional relationship between the leaf mass of 1.3 g, initial fall position of the leaf, and distance between the unadsorbed place and adsorption surface.

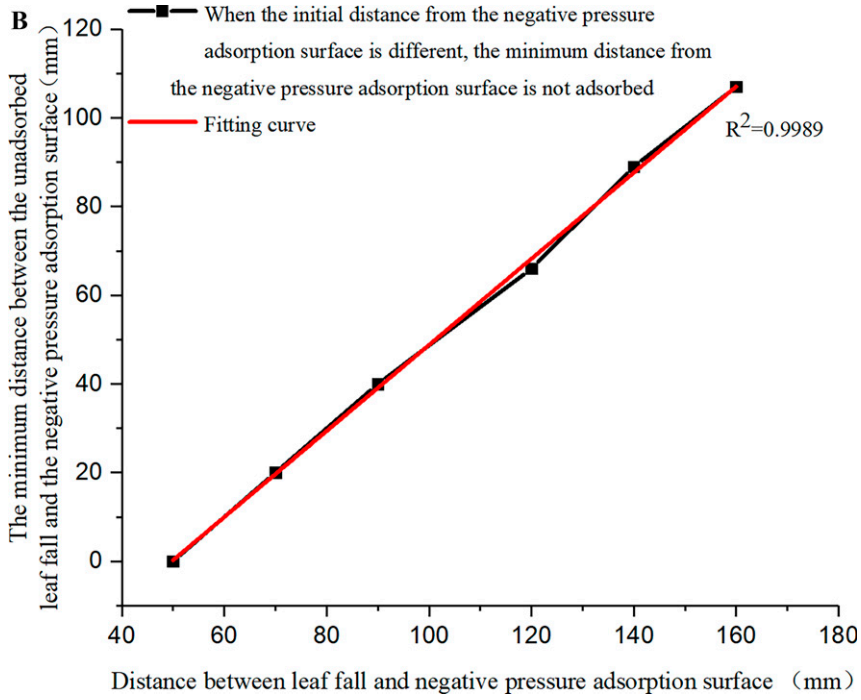


Fig. 11. Continued

away from the initial position of the negative pressure adsorption surface and were adsorbed by the negative pressure adsorption surface. As they fell closer to the initial position of the negative pressure adsorption surface, the adsorbed position of the particles also moved toward the upper end of the adsorption surface. The distances between the adsorbed position and the center of the adsorption surface were −80, −63, −48, −19, 0, and 19 mm, where ± indicates the direction, with the center of the adsorption surface as the origin, the upward direction was positive, and the downward direction was negative. It can be seen from the position coordinates that as the distance between the initial falling position of particles and the negative pressure adsorption surface became closer, the trajectory of particles being adsorbed was closer to the upper end of the negative pressure surface.

The initial distance between the leaf falling and the negative pressure adsorption surface was considered the x-axis, and the distance between the particle being adsorbed and the lower end of the adsorption surface was considered the y-axis. The corresponding coordinates of each position were (160 cm, 20 cm), (140 cm, 37 cm), (120 cm, 52 cm), (90 cm, 81 cm), (70 cm, 100 cm), and (50 cm, 119 cm), and function fitting was performed for each position point. In Fig. 12B, the fitting function expression was $y = 163.02 \pm 1.98 - (0.90 \mp 0.02)x$, and the adjusted $R^2$ of the fitting function was 0.9981. This showed that the fitted function (model) sufficiently captured the law in the data and had a strong ability to explain the change of the dependent variable. According to the fitting function, there was a relatively obvious linear correlation trend between the two variables studied. The negative slope of the fitting function indicated that the two variables were negatively correlated, that is, when the value of one variable increased, the value of the other variable tended to decrease, that is, at this mass, when the initial position of leaves falling from the negative pressure adsorption surface increased, the distance between the fall of the leaves and the bottom surface was smaller.

### Motion trajectory and analysis of leaves with mass of 0.1 g in a negative pressure flow field

Figure 13A shows the leaf mass of 0.1 g (magenta). When the leaf fell at different initial distances from the negative pressure adsorption surface, the distance between the particles and the center of the negative pressure adsorption surface was the distance between the particles being adsorbed, the center of the negative pressure adsorption surface was the distance between the particles being adsorbed, and the center of the adsorption surface was the upper end of the leaf mass at different initial distances. Their position values were 20, 30, 37, 50, 53, and 60 mm. The distance from the negative pressure center surface of the particles when adsorbed gradually increased with the decrease of the initial falling distance from the adsorption surface. For particles with a mass of 0.1 g, the longitudinal

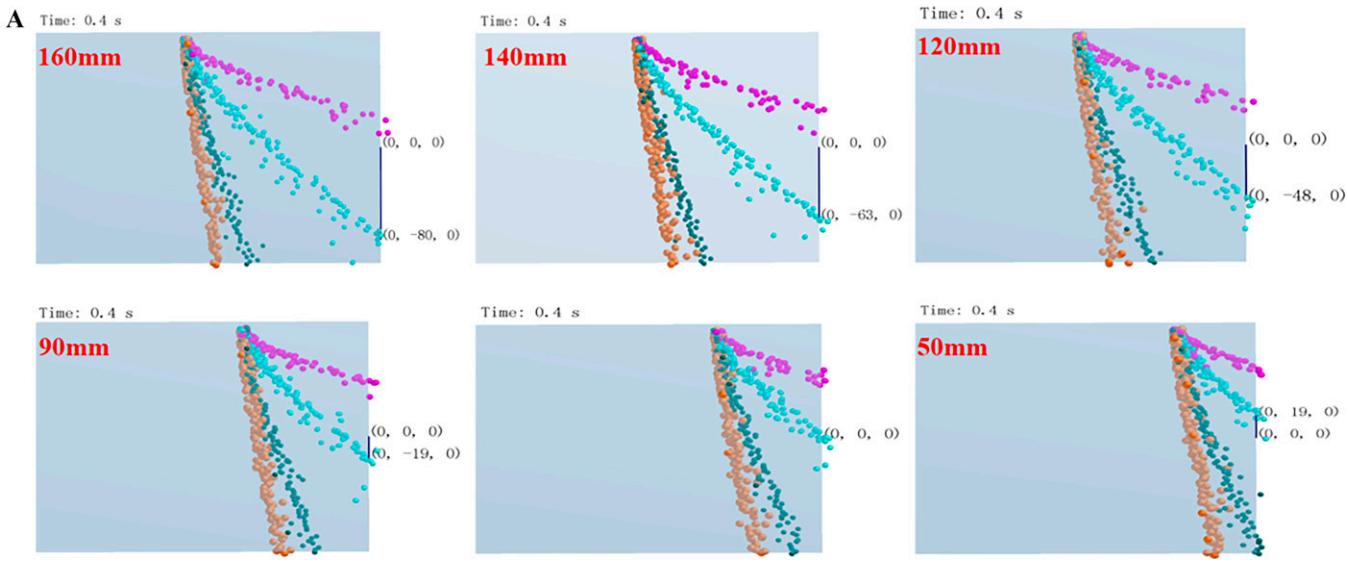


Fig. 12. (**A**) When the weight of leaves is 0.3 g and the initial distance between the falling position and negative pressure adsorption surface is different, the distance between the particles adsorbed and the center of the adsorption surface is different. (**B**) The mass of leaves is 0.3 g, and the relationship between the initial position of leaves at the beginning of falling and the distance between the adsorbed place and bottom end of the adsorption surface is a function.

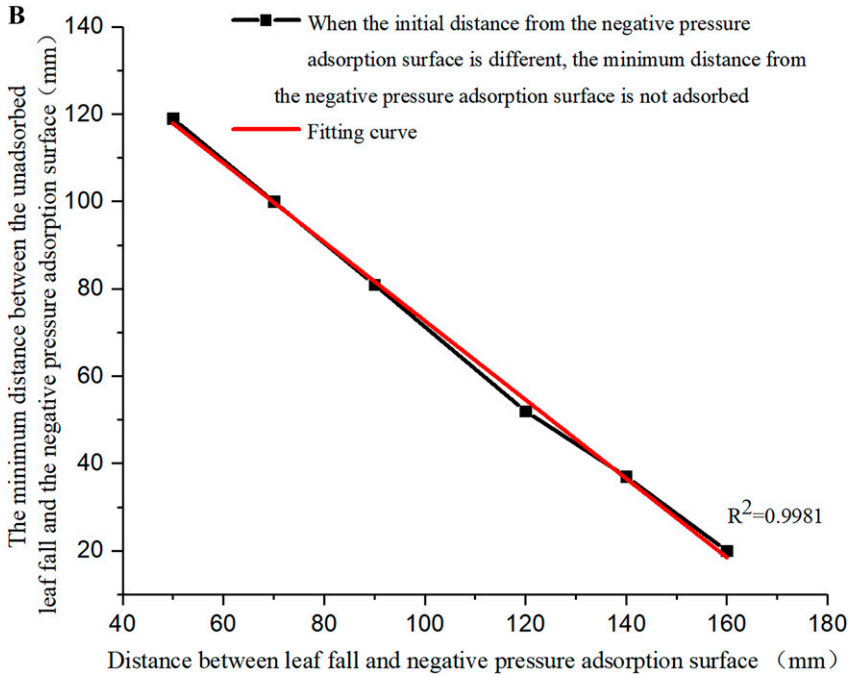


Fig. 12. Continued

adsorption spacing between particles was 10, 7, 3, and 7 mm when the initial falling position interval was 20 mm. Compared with particles with a mass of 0.3 g, the longitudinal adsorption spacing between particles were 17, 15, 19, and 19 mm when the initial falling position interval was 20 mm. The results showed that the change of the initial falling position had little effect on the change of longitudinal adsorption distance of 0.1-g particles.

The initial distance between the falling leaf and the negative pressure adsorption surface was considered the x-axis, and the distance between the particle being adsorbed and the central position of the adsorption surface was considered the y-axis. The corresponding coordinate points of each position were (160 cm, 20 cm), (140 cm, 30 cm), (120 cm, 37 cm), (90 cm, 50 cm), (70 cm, 53 cm), and (50 cm, 60 cm), and function fitting was performed for each position point. As shown in Fig. 13B, the fitting function expression was $y = 163.02 \pm 1.98 - (0.90 \mp 0.02)x$, and the adjusted $R^2$ of the fitting function was 0.9815. This showed that the fitted function (model) sufficiently captured the law in the data and had a strong ability to explain the change of the dependent variable. According to the fitting function, there was a relatively obvious linear correlation trend between the two variables studied. The negative slope of the fitting function indicated that the two variables were negatively correlated, that is, when the value of one variable increased, the value of the other variable tended to decrease. Under this mass, the initial position of the leaves falling from the negative pressure adsorption surface increased. The closer the falling distance of leaves was to the center of the negative pressure adsorption surface, the closer it was to the bottom of the negative pressure adsorption surface.

In summary, under the same negative pressure air field, leaves with different masses had different motion paths, but there was a certain regularity. In this airflow field, the distance between the falling position of the unadsorbed leaves and the bottom of the negative pressure adsorption surface was proportional to the initial distance between the falling position of the leaves and the negative pressure adsorption surface. The distance between the adsorbed leaves and the bottom of the negative pressure adsorption surface was inversely proportional to the initial distance between the fallen leaves and the negative pressure adsorption surface.

## Conclusion

Through the experimental analysis of the motion trajectory of multiscale flexible leaves adsorbed under the same negative pressure flow field, it was found that leaves with different mass significantly affected the motion trajectory of adsorbed leaves. Leaves with light mass were adsorbed after falling, and their motion trajectory was an approximate "L" shape; compared with leaves with heavy mass, their falling trajectory was approximately inclined and straight. The experiments

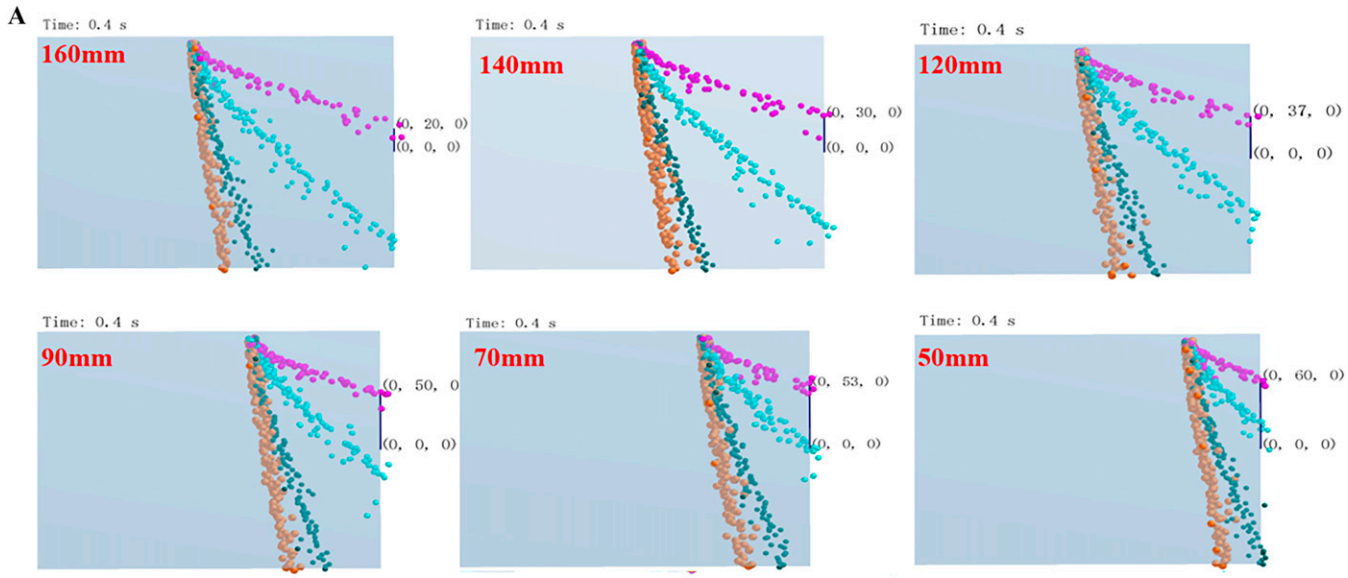


Fig. 13. (**A**) When the weight of leaves is 0.3 g and the initial distance between the falling position and negative pressure adsorption surface is different, the distance between the particles adsorbed and center of the adsorption surface is different. (**B**) The mass of leaves is 0.3 g, and the relationship between the initial position of leaves at the beginning of falling and the distance between the adsorbed place and bottom end of the adsorption surface is a function.

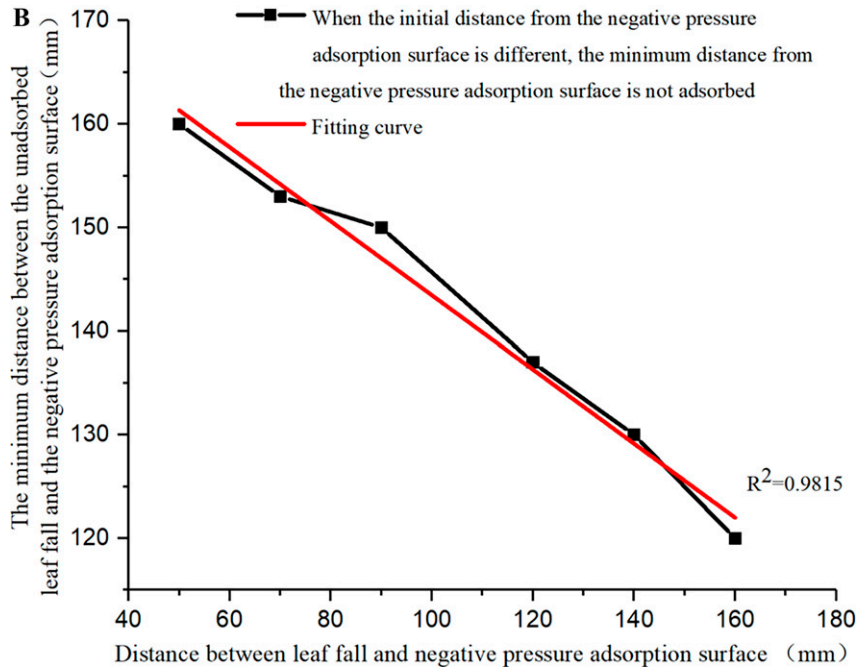


Fig. 13. Continued

provided basic data for studying the movement of leaves in the air flow field, guiding the optimization of the air suction device, and improving the sorting efficiency.

Based on the results of the experimental analysis and our previous research, a CFD-DEM coupling model of multiscale leaf movement under the same negative pressure flow field was established. The error between the simulation results and the experimental results of the model was less than 5%, which proved the applicability of the model. The model was used to analyze the multiscale leaf motion trajectory under the same negative pressure flow field and different initial distance from the leaf fall on the negative pressure adsorption surface. It was concluded that the distance between the fall position of the unadsorbed leaf and the bottom of the negative pressure adsorption surface was proportional to the initial fall distance. The distance between the adsorbed leaves and the bottom of the negative pressure adsorption surface was inversely proportional to the initial fall distance.

In summary, the research results provide a theoretical basis and data support for the optimal design and material sorting of air suction equipment in agricultural engineering and provide theoretical support for the later development of air suction sorting equipment for machine-picked tea leaves.

### References Cited


Chen GX, Liu WL, Liu CS, Zheng DQ, Yue LF. 2022. Simulation of airflow resistance and heat transfer characteristics of grain pile based on DEM-CFD. Chin J Grain Oil. 37(11):206–212. https://doi.org/10.20048/j.cnki.issn.1003-0174.000536.

Chen S. 2021. Simulation and optimization of key parameters of wheat harvester cleaning based on CFD-DEM (PhD Diss). Jinan University, Guangzhou, China. https://doi.org/10.27166/d.cnki.gsdcc.2021.000068.

Chen T, Yang HB, Yang JW, Lv D, Chen ZH, Wei QM. 2024. Numerical simulation and analysis of multi-phase flow in concrete mixing drum with CFD-DEM. Sci Technol Inf. 22(16):163–167. https://doi.org/10.16661/j.cnki.1672-3791.2403-5042-0579.

Cui T, Han DD, Yin XR, Li KH, Xiao LL, Yang L, Zhang DX. 2017. Design and experiment of Internal aerated blowing precision seed discharge device for maize. Trans Chin Soc Agric Eng. 33(1):9. https://doi.org/10.11975/j.issn.1002-6819.2017.01.002.

Fang M. 2022. Study on the particle motion characteristics and throwing mechanism of the disc knife chaff cutter on gas-solid coupling (PhD Diss). Inner Mongolia Agricultural University, Hohhot, China. https://doi.org/10.27229/d.cnki.gnmnu.2022.000050.

Gou DZ. 2021. CFD-DEM simulation of particle packing densification under gas impact conditions (PhD Diss). Northeastern University, Boston, MA, USA. https://doi.org/10.27007/d.cnki.gdbeu.2021.00141.

Jiang YZ, Hou XX, Zhao YM, Hu B, Luo X, Chen Y, Zhang H. 2019. Design and experiment of Air-suction drum precision seed discharging device for air-blown seed. J Gansu Agric Univ. 54(2):8.

Ji CY, Zhang C, Gu BX, Fu HQ, Xie D, Guo J. 2017. Design and experiment of comb-cutting air suction integrated tribute chrysanthemum picker. Trans Chin Soc Agric Machinery. 48(11):137–145. https://doi.org/10.6041/j.issn.1000-1298.2017.11.017.

Ju MK. 2022. Design and research of air-sucking Daylily harvesting system (PhD Diss). Shanxi Agricultural University, Shanxi, China. https://doi.org/10.27285/d.cnki.gsxnu.2022.000254.

Kong RR. 2023. Flow and heat transfer characteristics of ceramic heat carrier and biomass in a downcomer pyrolysis reactor based on CFD-DEM (PhD Diss). Shandong University of Technology, Shandong, China. https://doi.org/10.27276/d.cnki.gsdgc.2023.000257.

Li BH, Li H, Qi XD, Chen X, Ma YL, Wang YJ. 2021. Simulation and parameter optimization of seed dispenser based on CFD-DEM. J Intelligent Agric Equipment. 2(2):26–41. https://doi.org/10.12398/j.issn.2096-7217.2021.02.004.

Li DD, Wang RY, Zhu Y, Chen JN, Zhang G, Wu CY. 2024. Calibration of simulation parameters for fresh tea leaves based on the discrete element method. Agriculture. 14(1):148. https://doi.org/10.3390/agriculture14010148.

Li YH, Yang L, Zhang DX, Cui T, He XT, Du ZH. 2022. Performance analysis and structure optimization of high speed precision seed dispenser for air-sucking maize. Trans Chin Soc Agric Eng. 38:1–11. https://doi.org/10.11975/j.issn.1002-6819.2022.08.001.

Luo X, Hu B, Huang LL, Wang J. 2010. Design and experiment of precision planter for air-suction pot-pan seedling cultivation. Agric Mechanization Res. 32(11):130–132 + 140. https://doi.org/10.3969/j.issn.1003-188X.2010.11.033.

Mu ZQ, Yi SJ, Li YF, Mao X, Tao GX. 2022. Experimental study on the performance of air-suction corn precision seed dispenser. Agric Mechanization Res. 44(12):7.

Wu ZM. 2022. Research on tea classification algorithm and sorting equipment design and experiment (PhD Diss). Anhui Agricultural University. https://doi.org/10.26919/d.cnki.gannu.2020.000038.

Xiao Y. 2023. Research on seed absorption performance of sorghum grooved planter (PhD Diss). Guizhou University, Guiyang, China. https://doi.org/10.27047/d.cnki.ggudu.2023.001504.

Xie ZW. 2023. Study on dust diffusion law and numerical model of ventilation spray dust removal in tunnel construction by drilling and blasting method (PhD Diss). Chongqing University, Chongqing, China. https://doi.org/10.27670/d.cnki.gcqdu.2023.003529.

Xu MT, Chen K. 2022. Design and experiment of precision planter for air-suction pot tray breeding. Agric Mechanization Res. 44(1):161–164. https://doi.org/10.3969/j.issn.1003-188X.2022.01.028.

Yuan ZX, Dai F, Zhao WY, Shi RJ, Zhao YM, Xin SL. 2023. Simulation analysis and test of sifting device for flax air based on CFD-DEM. Agric Res DRY Areas. 41(6):281–290. https://doi.org/10.7606/j.issn.1000-7601.2023.06.30.

Zhang F. 2021. Research on particle movement and wear characteristics in centrifugal pump based on CFD-DEM (PhD Diss). Lanzhou University of Technology, Gansu, China. https://doi.org/10.27206/d.cnki.ggsgu.2021.000111.

Zhang K, Hong Y, Xu ZX. 2020. Simulation research of suction seed drain based on DEM-CFD coupling. J Nanjing Univ Inf Sci Technol: Nat Sci Edition. 12(6):767–772. https://doi.org/10.13878/j.cnki.jnuist.2020.06.01.

Zhang X, Zhu XY, Yu K. 2024a. Study on simulation and aspirated-air type experiment of fresh tea leaf with air suction based on CFD–DEM coupling. J Food Process Eng. 47(9):e14729. https://doi.org/10.1111/jfpe.14729.

Zhang X, Zhu X, Yu K, Wan J, Chen C. 2024b. Simulation and analysis of movement trajectories of fresh tea leaf particles based on CFD-EDEM coupling. J Food Process Eng. 47(7):e14692. https://doi.org/10.1111/jfpe.14692.

Zhang Y. 2024. Parameter optimization and experimental study of picking head of air suction small berry harvester (PhD Diss). Northeast Agricultural University, Harbin, China.

Zhao L. 2020. Simulation research and experiment of rice cleaning based on DEM-CFD coupling (MS Diss). University of Science and Technology Liaoning, Liaoning, China. https://doi.org/10.26923/d.cnki.gasgc.2020.000108.

Zhao XS, Yu FC, Zhao DW, Yu HL. 2020. Experimental study on performance of Air-suction precision seed discharge device for maize. J Agric Univ Hebei. https://doi.org/10.13320/j.cnki.jauh.2020.0102.

Zhou B. 2021. CFD-DEM simulation and experimental study on packing densification of cylindrical particles under gas impact (MS Diss). Northeastern University, Boston, MA, USA. https://doi.org/10.27007/d.cnki.gdbeu.2021.001811.